Intra-Patient Anatomic Statistical Models for Adaptive Radiotherapy

Stephen M. Pizer, Robert E. Broadhurst, Ja-Yeon Jeong, Qiong Han,
Rohit Saboo, Joshua Stough, Gregg Tracton, Edward L. Chaney

Medical Image Display & Analysis Group, University of North Carolina, Chapel Hill, NC, USA

***Abstract*— A statistical issue of clinical importance is intra-patient variation from day to day. We use these probability densities for segmentation of daily images by posterior optimization of deformable models. However, the information on intra-patient variation is only available after the multiple days of imaging; yet the densities are needed for segmentation on each day. Still, each patient's anatomy and image properties are distinct. We describe an approach of using sample means over the days so far to describe a Fréchet mean of the patient. We assume intra-patient variation is stationary across patients, so one can pool training statistics on residues from the mean of the respective patient. The approach is applied both to principal geodesic analysis of m-rep residues describing anatomic variation and to PCA of intensity quantile residues from model-relative regions. In trials to date, application of these statistics in segmentations of male pelvic organs from CT in adaptive radiotherapy yields results competitive with human segmentations and with segmentations based fully on intra-patient statistics.**

***Index Terms*— segmentation, adaptive radiotherapy, deformable model**

I. Introduction

Patients vary from day to day. In radiotherapy, which frequently takes place over tens of days, it is desirable to follow the changes in the target volume and in the organs to spare, so as to accommodate the treatment beams to these changes. In our methods the success of automatic segmentation of these organs on a treatment day depends on knowing both the patient's own anatomy and the variations in it from day to day, as well as that patient's image intensities in and near that organ and the variations in them from day to day. Clearly, the multi-day average of the geometric anatomy of a patient is specific to that patient, and the multi-day average of the images of that patient relative to the anatomy is specific to the physical properties of the tissues of that patient and also to the particular parameters of the imaging device used for that patient. These can be reasonably estimated from the images of a patient on the days so far (see [6] for one approach). However, satisfactory estimations of probability distributions on the inter-day variations of a target patient can be done only after most of the days of treatment. Instead we investigate the effectiveness of segmentation where these estimations assume stationarity across patients. This paper therefore covers ways of 1) producing sample means of the target patient's anatomy and image intensity information as the days pass and daily images are acquired and analyzed, 2) statistically analyzing the variation of changes from the respective patient mean in collections of other patients, and 3) applying these statistics in segmentation by posterior optimization of deformable models using the combination of within-patient sample means and other-patient statistics of variations.

Corresponding author: Stephen M. Pizer, email: pizer@cs.unc.edu. The work reported here was done under the support of NIH grant P01 EB02779.

Section 2 summarizes work by others on estimating inter-patient probability densities both on anatomic geometry and on intensities. It then describes our work on estimating these densities by Principal Geodesic Analysis (PGA) on m-rep geometric models and by PCA on regional intensity quantile functions (RIQFs), respectively. Section 3 describes the method for estimating intra-patient probability densities. Section 4 describes the application of these densities in the segmentation of intra-patient male pelvic organs from CT and gives results that show that segmentation by posterior optimization based on these probability densities gives results that are not only good but also as good as those given when the probability densities are estimated from all days of the particular patient.

II. Background

An atlas with variability can be understood as a probability density p_{anat} on anatomy $\underline{\mathbf{z}}$ together with a probability density $p_{img}(\mathbf{I}|\underline{\mathbf{z}})$ on image intensities relative to anatomy. Many have estimated p_{anat} using principal component analysis (PCA) on $\underline{\mathbf{z}}$ = landmarks ([7], [1]), on $\underline{\mathbf{z}}$ = boundary points ([8], [3], etc.), on $\underline{\mathbf{z}}$ = atlas diffeomorphisms [10], or on $\underline{\mathbf{z}}$ = implicit function representations ([15], [14]). We use a generalization of PCA called principal geodesic analysis (PGA) on an object representation called m-reps (Fig. 1) [12]. The most important properties of m-reps are that they represent the object interior and do so in terms that include local twisting, bending, and magnification and as such allow a rich description of the relations among parts of objects and among objects. Segmentation via probabilistic atlases has often been done by maximizing the likelihood [3], computing $arg\,max_{\underline{\mathbf{z}}}(p_{img}(\mathbf{I}|\underline{\mathbf{z}}))$. Instead, we do posterior optimization, computing $arg\,max_{\underline{\mathbf{z}}}(p_{img}(\underline{\mathbf{z}}|\mathbf{I})) = arg\,max_{\underline{\mathbf{z}}}[\log p_{anat}(\underline{\mathbf{z}}) + \log p_{img}(\mathbf{I}|\underline{\mathbf{z}})]$ [13]. Thus we depend on good estimation of the functions $\log p_{anat}(\underline{\mathbf{z}})$ and $\log p_{img}(\mathbf{I}|\underline{\mathbf{z}})$.

M-reps of simple objects (Fig. 1) consist of a sheet of medial atoms, with each atom consisting of a hub, given by its coordinates $\mathbf{p}$ and two equal-length spokes, given by their common length r and their respective directions (θ_1, ϕ_1) and (θ_2, ϕ_2), and with crest atoms having an extra bisecting spoke with its own length. We represent the sheet discretely by a grid (tuple) of these atoms [12]. In training p_{anat} for an object $\underline{\mathbf{z}}$, m-reps are fit to binary images [9]. Since medial atoms and thus tuples of them form a feature space that

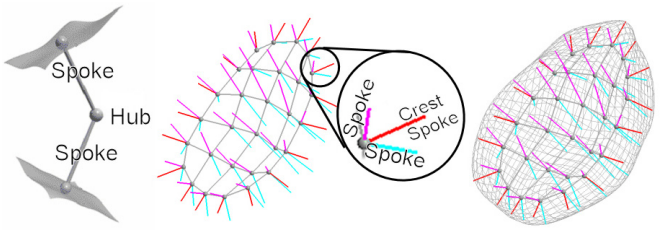

Fig. 1. A medial atom, a grid of medial atoms forming a discrete m-rep, and the implied boundary for a bladder.

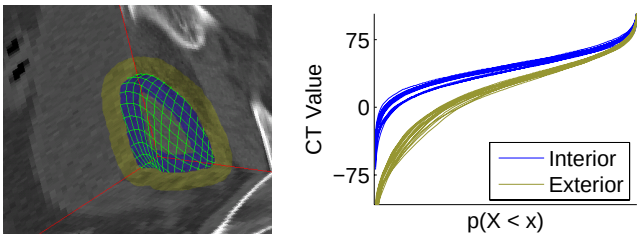

Fig. 2. Prostate image regions interior (blue) and exterior (yellow) to the boundary (mesh); their RIQFs on various days.

is curved, estimating probability densities of m-reps must use distances on this curved space. PGA [4] does this by estimating means by the Fréchet mean approach and writing residues (variation) $\Delta\underline{\mathbf{z}}$ from the mean as geodesic paths that become line segments with unchanged length when projected onto a tangent (flat) space at the Fréchet mean. PCA on these tangent-plane-projected residues is then applied, yielding $-2\log p_{anat}(\underline{\mathbf{z}})) = \sum_i \mathbf{a}_i^2/\sigma_i^2 +$ a constant, where $\mathbf{a}_i$ are $\Delta\underline{\mathbf{z}}$'s coefficients of the chosen principal vectors, and σ_i^2 are the corresponding principal variances.

By analogy to the above, we need a form of image intensity estimates to which we can both apply PCA and take residues from a mean. [2] has described an RIQF (Fig. 2) summarizing the intensities in an image region by sorting them, associating each intensity with a weight that monotonically decreases with distance from the m-rep boundary, dividing the list into quantiles (we use 200) with equal total weight, and representing the list by the 200-tuple $\mathbf{I}$ of quantile means. Because the set of affine changes of intensities produces a 2D subspace in the 200D feature space of these RIQFs, it is appropriate to do subtractions of RIQFs, take ordinary means of RIQFs, and do PCA on these RIQFs. Thus for each image region k we decompose the RIQF residue $\Delta\mathbf{I}^k \equiv \mathbf{I}^k -$ its mean $\bar{\mathbf{I}}^k$ into the chosen principal directions. Using K regions that have independent intensity distributions, e.g., a region interior to the object and a region exterior to that object, yields $-2\log p_{img}(\mathbf{I}|\underline{\mathbf{z}}) = \sum_{k=1}^{K}\sum_i {b_i^k}^2/{\tau_i^k}^2 +$ a constant, where b_i^k are the $\Delta\mathbf{I}^k$'s projections onto the k^{th} region's chosen principal modes and their residue space (the region depends on the vector $\mathbf{a}$), and ${\tau_i^k}^2$ are the corresponding principal variances. (Per [2] bowel gas and bone intensities are handled separately.) Posterior maximization thus amounts to minimizing $\sum_i \mathbf{a}_i^2/\sigma_i^2 + \sum_{k=1}^{K}\sum_i {b_i^k}^2/{\tau_i^k}^2$ over $\mathbf{a}$.

III. Method

Patient mean. On day j we need a target patient mean over days 1 through $j-1$. For anatomy this must be the Fréchet mean $\bar{\mathbf{z}}^j$ of those days' m-reps, appropriately aligned. Similarly, a patient mean of the object-relative intensity data is computed as the collection, over k, $\bar{\mathbf{I}}^{kj}$ of mean regional quantile tuples over the first $j-1$ days. For training patients, all days are available, so the means are taken over all days for each respective patient.

Estimating residue probability distributions. We model aligned residues from a patient mean, $\Delta\underline{\mathbf{z}}$ and $\Delta\mathbf{I}$ for any region, as probabilistically stationary. Thus we pool the residues of each type, over all days and patients. The respective probability densities can be estimated by PGA and PCA respectively on pooled residues. Thus $\bar{\mathbf{z}}^j$, the $\bar{\mathbf{I}}^{kj}$, and the collection of probability densities from the pooled residues form the patient-specific atlas.

A target patient is described as the mean over the patient days to date + a residue. The sample mean and residue are independent random variables. If the pooled covariance matrices of the residues $\Delta\underline{\mathbf{z}}$ and the $\Delta\mathbf{I}^k$ are $\Sigma_{\Delta\underline{\mathbf{z}}}$ and $\Sigma_{\mathbf{I}^k}$, respectively, the covariance matrix of the sample mean = $1/(j-1)$ times the respective Σ. Therefore, the covariance for the target patient description is $j/(j-1)\times$ the respective Σ. Since this holds for both the $-2\log p_{anat}(\underline{\mathbf{z}})$ term and the $-2\log p_{img}(\mathbf{I}|\underline{\mathbf{z}})$ term in the $-2\log$ posterior being optimized, the log posterior need not be adjusted for j.

IV. Segmentation Experiments and Results

We did two experiments on segmenting prostates and bladders from male pelvis CTs in 6 patients (86 images). To study the effectiveness of our pooling method, we successively left each patient out, trained on 5 remaining patients pooled, and segmented the left-out patient as described above. To provide a baseline for the effectiveness of this method, we trained each patient independently on a leave-one-day-out basis.

Fig. 3 shows the RIQF mean and first principal mode of variation for a target patient from both intra-patient training and other patient training. The first two principal modes for other patient training cover 95.2% (interior) and 90.0% (exterior) of the variability of the target patient. This can be compared to the first two principal modes of intra-patient training on the target patient, which cover 96.7% (interior) and 97.4% (exterior) of the variability of that patient.

For the majority of cases, the segmented results for both the bladder and prostate were judged qualitatively good. Typical cases from two patients are displayed in 3D in Figs. 4 and 5. Typical cases from all six patients against sagittal slices in the middle of the prostate and bladder are displayed in Fig. 7. These segmentations were done organ by organ, allowing prostate-bladder overlaps, but other methods from our laboratory reflect inter-organ relations in the segmentation [5]. Sorted statistics over all 86 images for both experiments are given in Fig. 6. For comparison, m-rep fits to humans average ∼93%, and the average agreement between two humans' segmentations of 16 prostates is 81% volume overlap, 1.9mm average closest point surface separation.

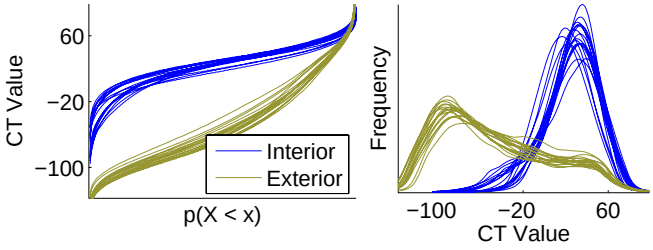

(a) A single patient's Bladder RIQFs

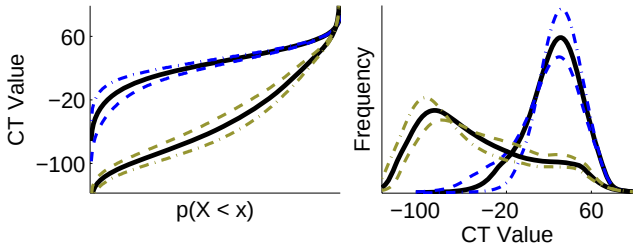

(b) Intra-patient training

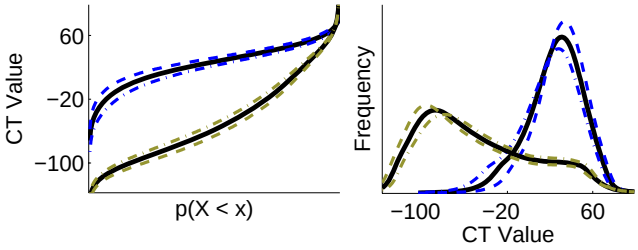

(c) Other patient training

Fig. 3. Comparison of intra-patient and other patient training of bladder RIQFs. (a) a patient's interior and exterior daily bladder RIQFs (left) and their histogram representation (right). (b) the mean and ± 2 std. devs. along the first principal component both learned from all of the images of this patient. (c) the mean learned from this patient and ± 2 std. devs. along the first principal component learned from the other 5 patients.

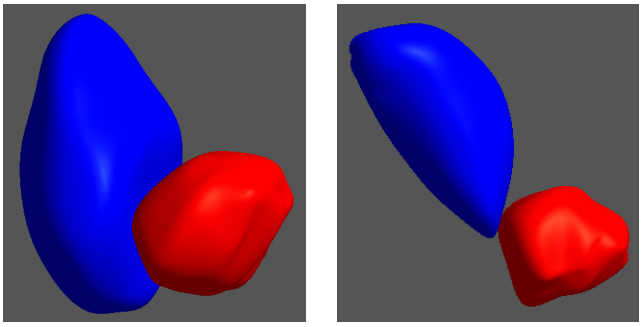

Fig. 4. Bladder (blue) and prostate (red) 3D segmentations from two patients shown from a sagittal perspective.

The measures given in Fig. 6 suggest that performance in the pooled approach is comparable with the baseline approach and is competitive with human segmentations. The latter conclusion is limited by the fact that this experiment was done by optimizing the tuple of m-rep atoms for the organ in question only as a whole. The second stage of our full algorithm, optimizing each atom individually, has not yet been applied here. Thus in certain high-contrast regions our present results are noticeably a voxel or two off. We expect tight

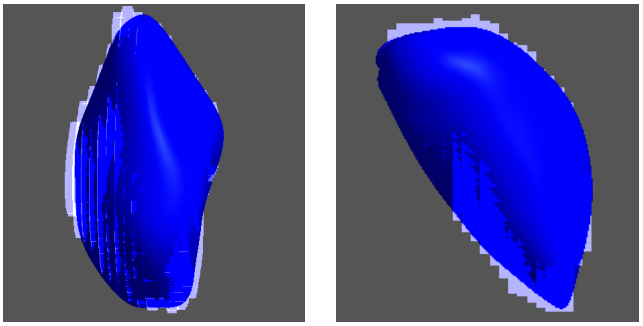

Fig. 5. Two bladder segmentations shown with the corresponding human segmentations in light blue.

agreement there when we apply the atom optimization stage.

Acknowledgements

The authors are grateful to Julia Fielding, Julian Rosenman, and Di Yan for images and image segmentations. We thank Xifeng Fang, Graham Gash, Sarang Joshi, Joshua Levy, Derek Merck, and Keith Muller for conceptual, algorithmic, code, and operations contributions.

References

[1] F.L. Bookstein, *Morphometric Tools for Landmark Data: Geometry and Biology*, Cambridge University Press, 1991.

[2] R.E. Broadhurst, J Stough, S.M. Pizer, and E.L. Chaney, "A statistical appearance model based on intensity quantiles," 2006 *IEEE International Symposium on Biomedical Imaging* (*ISBI*), pp. 422-425.

[3] T.F. Cootes, G.J. Edwards, C.J. Taylor , "Active appearance models," in *Proc. European Conference on Computer Vision* (*ECCV*) 1998, Vol. 2, pp. 484-498, Springer, 1998.

[4] P.T. Fletcher, C. Lu, S.M. Pizer, and S. Joshi, "Principal geodesic analysis for the study of nonlinear statistics of shape," *IEEE Trans. Medical Imaging*, Vol. 23 (8), pp. 995-1005, 2004.

[5] J-Y Jeong, S.M. Pizer, S. Ray, "Statistics on anatomic objects reflecting inter-object relations", *Proc. Workshop on Mathematical Foundations of Computational Anatomy, MICCAI* 2006.

[6] Y. Jeong, and R.J. Radke, "Modeling inter- and intra-patient anatomical variation using a bilinear model," in Proc. *Mathematical Methods in Biomedical Image Analysis* (*MMBIA*), 2006 IEEE Computer Vision and Pattern Recognition workshop.

[7] D. Kendall, "A survey of the statistical theory of shape", *Statistical Science*, Vol. 4 (2), pp. 87-120, 1989.

[8] T. McInerny, and D. Terzopoulos, "Deformable models in medical image analysis: a survey," *Medical Image Analysis*, Vol. 1 (2), pp. 91-108, 1996.

[9] D. Merck, G. Tracton, S.M. Pizer, and S. Joshi (2006), "A methodology and implementation for constructing geometric priors for deformable shape models." Available: http://midag.cs.unc.edu/MIDAG_FS.html

[10] M. Miller, A. Banerjee, G. Christensen, S. Joshi, D. Khaneja, U. Grenander, and L. Matejic, L, "Statistical methods in computational anatomy," *Stat. Methods in Medical Research*, Vol. 6, pp. 267-299, 1997.

[11] X. Pennec, "Probabilities and statistics on Riemannian manifolds: basic tools for geometric measurements," in *IEEE Workshop on Nonlinear Signal and Image Processing*, 1999.

[12] S.M. Pizer, P.T. Fletcher, S. Joshi, A. Thall, Z. Chen, Y. Fridman, D. Fritsch, et al., "Deformable m-reps for 3D medical image segmentation," *International Journal of Computer Vision*, Vol. 55, pp. 85-106, 2003.

[13] S.M. Pizer, M. Styner, et al., "Statistical applications with deformable m-reps," Chapter 9 in K. Siddiqi, S.M. Pizer, *Medial Representations, Algorithms and Applications*, Springer, to appear, 2006.

[14] A. Tsai, W. Wells, C. Tempany, E. Grimson, and A. Willsky, "Coupled multi-shape model and mutual information for medical image segmentation," *Information Processing in Medical Imaging*, LNCS 2732, pp. 185-197, Springer, 2003.

[15] J. Yang, L.H. Staib, J.S. Duncan, "Neighbor-constrained segmentation with 3D deformable models," *Information Processing in Medical Imaging*, LNCS 2732, pp. 198-209, 2003.

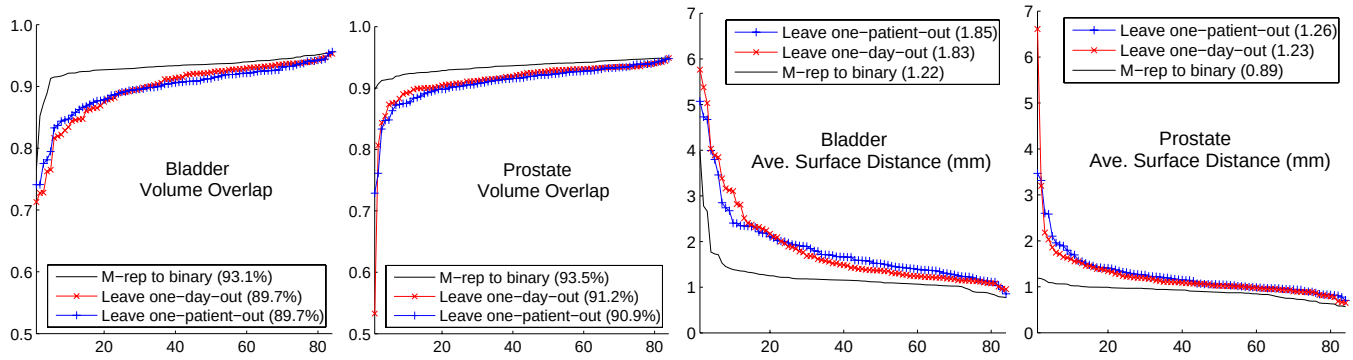

Fig. 6. Sorted measures comparing human segmentations to m-rep segmentations and m-rep fits into the human's, over 86 images. Averages are in parentheses.

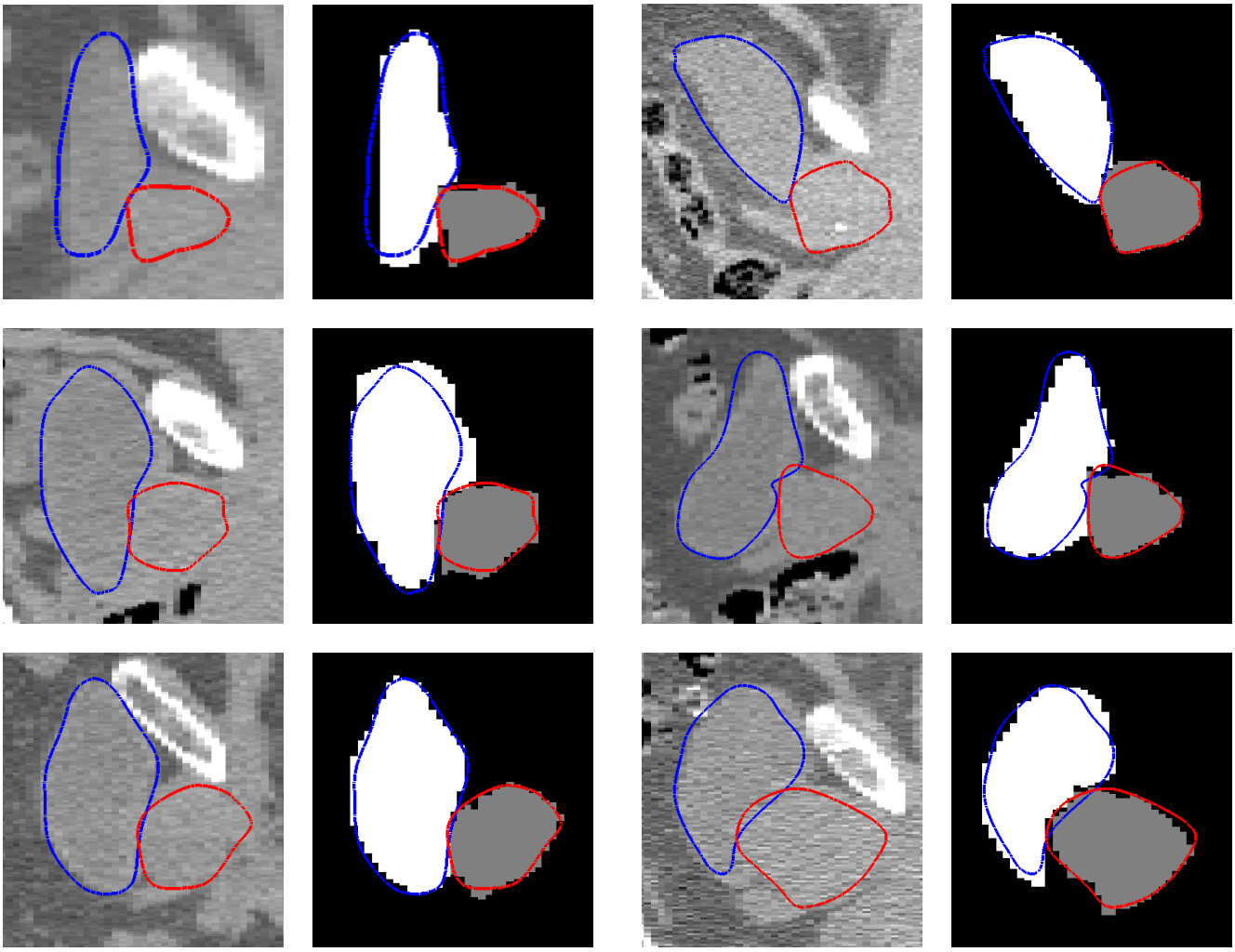

Fig. 7. Typical automatic segmentations for each patient. Bladder (blue) and prostate (red) contours, shown on a central sagittal slice on the CT image (left) and the corresponding manual segmentation (right).